

## Correlation-induced valley splitting and orbital magnetism in a strain-induced zero-energy flatband in twisted bilayer graphene near the magic angle

Yu Zhang,<sup>1,\*</sup> Zhe Hou,<sup>2,\*</sup> Ya-Xin Zhao,<sup>1</sup> Zi-Han Guo,<sup>1</sup> Yi-Wen Liu,<sup>1</sup> Si-Yu Li,<sup>1,3</sup>  
Ya-Ning Ren,<sup>1</sup> Qing-Feng Sun,<sup>2,4,5,†</sup> and Lin He<sup>1,‡</sup>

<sup>1</sup>Center for Advanced Quantum Studies, Department of Physics, Beijing Normal University, Beijing 100875, People's Republic of China

<sup>2</sup>International Center for Quantum Materials, School of Physics, Peking University, Beijing 100871, People's Republic of China

<sup>3</sup>Key Laboratory for Micro-Nano Physics and Technology of Hunan Province, College of Materials Science and Engineering, Hunan University, Changsha 410082, People's Republic of China

<sup>4</sup>Collaborative Innovation Center of Quantum Matter, Beijing 100871, People's Republic of China

<sup>5</sup>Beijing Academy of Quantum Information Sciences, West Bld. #3, No. 10 Xibeiwang East Road, Haidian District, Beijing 100193, People's Republic of China

 (Received 13 March 2020; revised 11 August 2020; accepted 12 August 2020; published 24 August 2020)

In the vicinity of the magic angle in twisted bilayer graphene (TBG), many exotic correlated states, such as superconductivity, ferromagnetism, and topological phases, are observed because the two low-energy Van Hove singularities (VHSs) become exceedingly narrow, i.e., become flatbands. Heterostrain, strain in van der Waals structures where each layer is strained independently, can modify the single-particle band structure of the TBG and lead to various properties. Here, we show that heterostrain in a TBG near the magic angle generates a zero-energy flatband between the two VHSs. Doping the TBG to partially fill the zero-energy flatband, we observe a correlation-induced valley-polarized gap of  $\sim 10$  meV. By applying perpendicular magnetic fields, a large and linear response of the gap to magnetic fields is observed, attributing to the large orbital magnetic moments in TBG. The measured orbital magnetic moment per moiré unit cell is  $\sim 15 \mu_B$  in the TBG, which is well consistent with our calculations.

DOI: [10.1103/PhysRevB.102.081403](https://doi.org/10.1103/PhysRevB.102.081403)

In electronic flatbands, the kinetic energy of the charge carriers is quenched and electron-electron interactions may lead to the strongly correlated phases. A celebrated example is the appearance of low-energy flatbands in magic-angle twisted bilayer graphene (TBG) [1–10]. When the twist angle is finely tuned to the “magic angle,” the low-energy Van Hove singularities (VHSs) in the TBG become exceedingly narrow, i.e., become flatbands [7–10], and many exotic correlated phases are observed in experiments very recently [11–16]. An alternative route to realize the flatbands in a two-dimensional membrane is to introduce strain. Previous studies show that a slight strain in graphene can not only reshape the Brillouin zone and reduce the symmetry of lattice, but can also introduce an additional scalar and gauge potentials due to the modified electron-hopping amplitudes [17–35]. The gauge potential acts as a pseudomagnetic field on the Dirac electrons and is expected to generate pseudo-Landau levels (flatbands) [17–35], which are predicted to introduce correlated phases quite different from the VHSs in the magic-angle TBG [36]. However, there is no experimental evidence of many-body correlations in the strain-induced flatbands

of graphene up to now. In this Rapid Communication, we demonstrate that TBG near the magic angle with heterostrain, i.e., each layer is strained independently due to the weak interlayer coupling [37], can generate a new zero-energy flatband between the two low-energy VHSs. Our experiments show clear evidence of strongly electron-electron correlations in the strain-induced zero-energy flatband. Valley-polarized ground state and correlation-induced orbital magnetism are clearly observed when the zero-energy flatband is partially filled.

In our experiments, large-area aligned graphene monolayer was grown on copper foils via a chemical vapor deposition method and the aligned graphene monolayer was cut into two pieces to fabricate the TBG with a target twist angle  $\theta$  [38,39]. Then, the obtained TBG was transferred onto a SiO<sub>2</sub>/Si wafer covered by a Bernal-stacked bilayer graphene, as schematically shown in Fig. 1(a) (see Methods and Supplemental Material Figs. S1–S3 [40]). The Bernal-stacked bilayer graphene can efficiently reduce electronic inhomogeneities of the TBG arising from the SiO<sub>2</sub>/Si substrate. The twist angle between the TBG and the supporting Bernal-stacked bilayer graphene is larger than 10° to ensure that they are electronically decoupling. By using the back-gated device and scanning tunneling microscope (STM), as shown in Fig. 1(a), we can systematically study the electronic properties of the TBG as a function of carrier density. Figure 1(b) shows a representative STM topographic image of the TBG, which exhibits a moiré superlattice with the bright spots

\*These authors contributed equally to this work.

†Author to whom correspondence should be addressed: [sunqf@pku.edu.cn](mailto:sunqf@pku.edu.cn)

‡Author to whom correspondence should be addressed: [helin@bnu.edu.cn](mailto:helin@bnu.edu.cn)

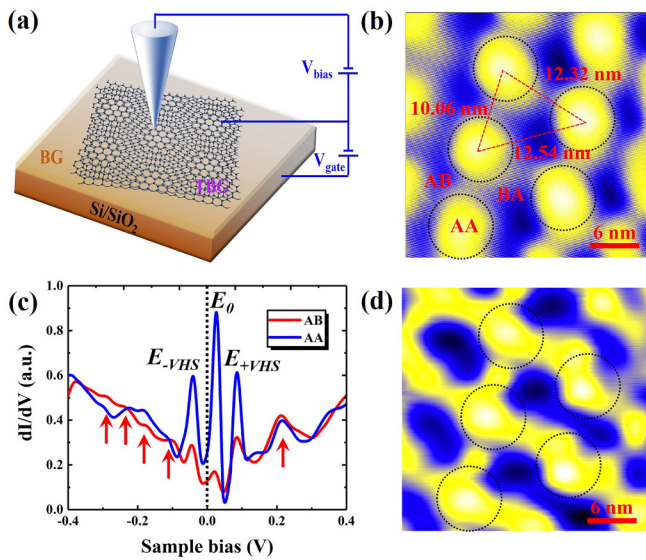


FIG. 1. (a) Schematic of the STM setup on the TBG devices. (b) A  $30 \times 30 \text{ nm}^2$  STM topographic image showing the moiré superlattice with a twist angle  $\theta \sim 1.2^\circ$  and heterostrain  $\varepsilon \sim 0.38\%$  ( $V_b = 300 \text{ mV}$ ,  $I = 0.2 \text{ nA}$ ). (c) Typical STS spectra recorded at AA and AB regions ( $V_b = 300 \text{ mV}$ ,  $I = 0.2 \text{ nA}$ ). Peaks of  $E_0$  and  $E_{\pm VHS}$  are marked in the figure. The black dashed line is the energy of the Fermi level. (d) A typical STS map recorded at the energy of  $E_0$ . The black dotted circles mark the period and circular symmetry of the AA regions of the moiré patterns in the TBG.

corresponding to the AA stacking regions and the dark regions consisting of alternating AB/BA stacking regions [41–45]. The periods of the moiré pattern along the principal directions exhibit obvious anisotropy, indicating that there is a small amount of heterostrain in the TBG. Such a heterostrain is frequently observed and almost unavoidable in TBG [37,41–46]. It mainly originates from the annealing process due to the mismatch of thermal expansion coefficients between graphene and the supporting substrates [47], as well as the sample transfer techniques [43] in our experiments. A detailed Fourier analysis of the moiré lattice reveals that the twist angle of the TBG is  $(1.198 \pm 0.013)^\circ$ , which is close to the magic angle ( $\sim 1.1^\circ$ ), and there is a slight heterostrain that consists of both a small uniaxial heterostrain  $\varepsilon_{\text{uni}}^{\text{het}} = (0.38 \pm 0.02)\%$  along the horizontal direction and an even smaller biaxial heterostrain  $\varepsilon_{\text{bi}}^{\text{het}} = -0.05\%$  in the TBG that are uniform within the area of  $500 \times 500 \text{ nm}^2$  (Figs. S4–S6 [40]). Such a precise determination of the strain and twist angle is attributed to the moiré pattern that can serve as a magnifying glass to zoom-in the heterostrain in the TBG [37,41–46].

Figure 1(c) shows two typical  $dI/dV$  spectra measured at the AA and AB regions of the TBG. The spectra feature three sharp peaks (labeled as  $E_{-VHS}$ ,  $E_{+VHS}$ , and  $E_0$ ), which are much more intense in the AA regions. To explore the nature of these peaks, we carried out the scanning tunneling spectroscopy (STS) maps, which can directly reflect the spatial distributions of the local density of states (LDOS), at the energies of these peaks (Fig. S7 [40]). Our measurement demonstrates that the electronic states of the three peaks are mainly localized in the AA regions of the moiré pattern, as

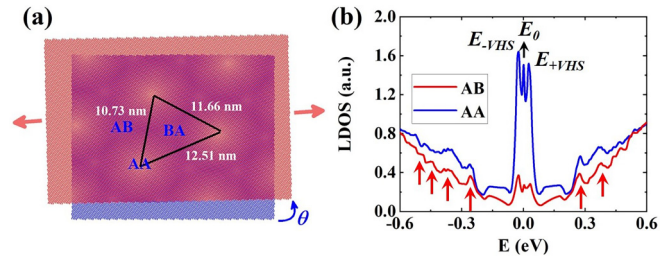


FIG. 2. (a) Schematic of the TBG with the twist angle  $\theta$  and a uniaxial strain applied to the above layer only. The calculated moiré periods are given in the figure. (b) The LDOS in the AA and AB stacked regions obtained from the tight-binding model. Peaks of  $E_0$  and  $E_{\pm VHS}$  are marked in the figure. The strain-induced pseudo-Landau levels of massive Dirac fermions are marked by the arrows.

shown in Fig. 1(d) as an example, which exhibits the same structure as the moiré pattern. Usually, there are two low-energy VHSs flanking the charge neutrality point in slightly TBG and the two VHSs are mainly localized in the AA regions of the moiré pattern [1–7,41–44]. Therefore, the two peaks flanking the  $E_0$  are attributed to the two VHSs of the TBG. The  $E_0$  peak around the charge neutrality point is attributed to the flatband that is generated by the heterostrain in the TBG. Very recently, it was demonstrated explicitly that the heterostrain can efficiently reconstruct the band structure and introduce a flatband between the two VHSs of a  $1.25^\circ$  TBG [37], indicating that the zero-energy flatband can appear in the TBG within a wide range of heterostrain. To further confirm the origin of  $E_0$ , we carry out tight-binding calculation by considering the heterostrain of the TBG, as shown in Fig. 2 (see Supplemental Material for details [40]). There are three low-energy peaks, which are mainly localized in the AA regions, in the LDOS of the TBG, and the heterostrain in the TBG generates a zero-energy flatband between the two VHSs. Obviously, our theoretical results reproduce the main feature of our experimental observation. In our experiment, the energy separation between the two VHSs,  $\sim 120 \text{ meV}$ , of the TBG is much larger than that obtained in theory,  $\sim 50 \text{ meV}$ . The giant enhanced energy separation between the VHSs is attributed to the strong  $e-e$  interactions when the chemical potential lies between the two VHSs. Very recently, similar behavior has been observed in the magic-angle TBG and is treated as evidence for the strong many-body correlations in the magic-angle TBG [41–44].

The other notable feature in Fig. 1(c) is the appearance of several weak peaks at high energies, as marked by the red arrows (Fig. S8 [40]). These peaks are attributed to strain-induced pseudo-Landau levels in the TBG. The strain generates pseudomagnetic fields that confine the massive Dirac electrons into circularly localized pseudo-Landau levels, as demonstrated very recently in low-angle TBG [45,46]. In our experiments, the values of pseudomagnetic fields vary from 16.5 to 35.6 T, which are attributed to the heterostrain that is periodically tuned by the moiré superlattice (Fig. S9 [46]). Our theoretical calculation also demonstrates that the heterostrain can generate high-energy peaks in the DOS of the TBG, as shown in Fig. 2(b). The energy spacing between the pseudo-Landau levels obtained in theory is slightly larger

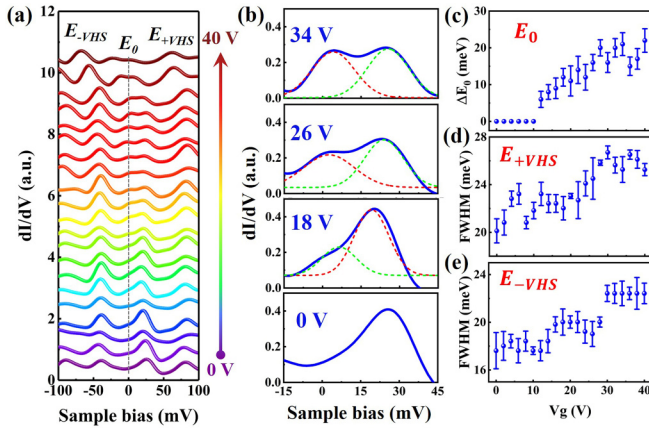


FIG. 3. (a) STS spectra recorded in the center of the AA region of the TBG as a function of back-gate voltages from 0 to 40 V (the step size in gate voltage is 2 V). When the back-gate voltage is 0 V, the strain-induced flatband  $E_0$  is empty. With increasing the back-gate voltage to 40 V,  $E_0$  is almost half filled and splits into two peaks flanking the Fermi level. The gray dashed line is the energy of the Fermi level, and all the curves are offset for clarity. (b) Typical high-resolution STS spectra of  $E_0$  measured under different back-gate voltages. The dashed lines mark the results of Gaussian fitting for the split  $E_0$ . (c)–(e) The energy separations of the splitting  $E_0$  and the FWHM of  $E_{+VHS}$  ( $E_{-VHS}$ ) as a function of  $V_g$ .

than that measured in experiment, which may arise from a relatively larger strain-induced pseudomagnetic field of the TBG in our simulation.

In our studied TBG, the kinetic energy of electrons in the strain-induced flatband can be estimated by the bandwidth as  $W_0 = 16.8$  meV [11,48], which is much smaller than the on-site Coulomb energy of each site  $U \sim e^2/\epsilon L \sim 27$  meV ( $e$  is the electron charge,  $\epsilon \sim 4.4$  is the estimated dielectric constant of the device in our experiments [49–51], and  $L \sim 12$  nm is the moiré period) [11]. Therefore, bringing the Fermi energy within the strain-induced flatband is expected to lead to various strongly correlated phases. To explore this, we measure the properties of the TBG as a function of electron density in the back-gated devices. Figure 3(a) shows representative  $dI/dV$  spectra measured on the AA regions of the moiré pattern in the TBG as a function of back-gate voltage  $V_g$ . When  $0 \text{ V} < V_g < 12 \text{ V}$ , the strain-induced flatband  $E_0$  is fully unoccupied and the tunneling spectrum is almost independent of  $V_g$ . However, when we continuously increase the back-gate voltage ( $V_g > 12 \text{ V}$ ) and  $E_0$  becomes partially filled, a notable new feature is observed in the spectra:  $E_0$  splits into two peaks, as delicately demonstrated in Fig. 3(b). Figure 3(c) summarizes the splitting of  $E_0$  as a function of  $V_g$ . Simultaneously, we observe a slight broadening of both the fully occupied VHS and the completely empty VHS when the strain-induced flatband is partially filled, as shown in Figs. 3(d) and 3(e). The full width at half maximum (FWHM) of the two VHSs increases simultaneously with the splitting of the flatband. Such a phenomenon is unexpected since there is no reason to expect a broadening of the fully occupied (or completely empty) bands when the occupation of the other bands is changed. The above two features are quite similar to the strong many-body correlations observed in the

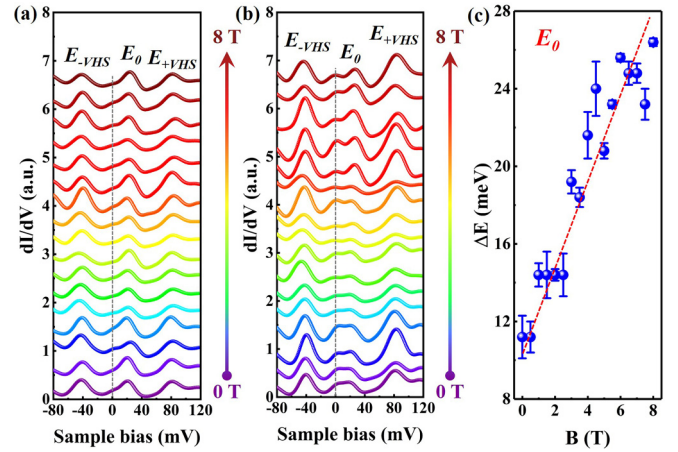


FIG. 4. (a) Typical STS spectra measured in different magnetic fields when the strain-induced flatband is empty. (b) High-resolution STS spectra measured in different magnetic fields when the strain-induced flatband is partially filled. The gray dashed line is the energy of the Fermi level, and all the curves are offset for clarity. (c) Energy separations of the two split peaks as a function of magnetic fields. The red dashed line is the linear fit.

magic-angle TBG [41–44]. In the magic-angle TBG, when one of the VHSs is partially filled, both a correlation-induced gap of about 10 meV in the partial-filled flatband [41–44] and a broadening of the other flatband [41] are also observed. This indicates that the  $e$ - $e$  interactions are also very important in the strain-induced flatband and, therefore, it is possible to realize interesting correlated phenomena in this system.

Although the correlation-induced gap is clearly observed in this work and in the magic-angle TBG when the flatband is partially filled, the nature of the gap observed in the STM measurements [41–44] is still unclear up to now. A careful examination of the back-gate-dependent spectra in Fig. 3(a) reveals that the  $e$ - $e$  interactions prefer to split the DOS peak of the partially filled flatband  $E_0$  into two subpeaks with equal intensities. Because of the fourfold spin-valley flavor degeneracies and weak spin-orbital coupling in graphene, this symmetry-breaking state indicates that either the spin or valley degeneracy of the flatband is lifted by the  $e$ - $e$  interactions. To further explore the nature of the splitting, we measure high-resolution STS spectra of the TBG in different doping levels as a function of perpendicular magnetic fields, as summarized in Fig. 4. The tunneling spectra are almost independent of the magnetic fields when the strain-induced flatband is completely empty, as shown in Fig. 4(a). However, when the flatband is partially filled, the correlation-induced splitting increases quickly with increasing the magnetic fields, as shown in Fig. 4(b) (see Fig. S10 for details [40]). Figure 4(c) shows the splitting  $\Delta E$  as a function of magnetic field, which exhibits a linear scaling. A linear fit of the experimental data to a Zeeman-like splitting  $\Delta E = 2g^* \mu_B B$  yields  $g^* \approx 15$ , which helps us directly rule out the spin splitting since the  $g^*$  for the electron spin is only 2. Such a large  $g^*$ , which is almost the same as that of the valley splitting in graphene monolayer when the zero Landau level is half filled [52–54], reminds us of the valley splitting in the strain-induced flatband.

Theoretically, the spontaneously valley-polarized ground state at the partial-filled flatbands is energetically favored with considering the  $e$ - $e$  interactions [55–61]. It was predicted that when the valley degeneracy of the flatband is lifted by the  $e$ - $e$  interactions and the  $C_{2z}$  symmetry of the TBG is broken by the substrate, each valley would be associated with nonvanishing Berry curvature. Then, a large orbital magnetic moment and nonzero valley Chern numbers can be generated in the TBG [58–69]. In this case, a large linear response of energy splitting to the magnetic fields is supposed to be observed because of the coupling of the orbital magnetic moments to the magnetic field [58,59,65]. In our experiment, the  $e$ - $e$  interactions lead to the valley splitting of  $\sim 10$  meV in the strain-induced flatband, and the supporting Bernal bilayer graphene can efficiently break the  $C_{2z}$  symmetry of the TBG. Therefore, a large orbital magnetic moment is expected to emerge in this system and the orbital magnetic moment in each moiré of the TBG is estimated as  $\sim 15\mu_B$ , according to the obtained slope in Fig. 4(c). To better apprehend such a large orbital magnetic moment, we carry out the quantitative calculations in the TBG from the continuum model [7,30,69]. Our calculations show that the orbital magnetic moment in this system is  $\sim 2.8\mu_B$  per moiré unit cell per electron, as explicitly demonstrated in Figs. S11 and S12 of the Supplemental Material [40]. For the half-filling zero-energy flatband, i.e., the Fermi energy locates at the charge neutrality point, there are four electrons occupying each moiré unit cell. Therefore, the theoretically

acquired orbital magnetic moment is  $\sim 11.2\mu_B$  per moiré unit cell, which is well consistent with our experiment.

In summary, we demonstrate explicitly that the strong  $e$ - $e$  correlations dominate the electronic properties in the strain-induced zero-energy flatband in TBG near the magic angle. The  $e$ - $e$  interactions lift the valley degeneracy of the strain-induced flatband and lead to a large orbital magnetic moment of  $15\mu_B$  in each moiré when the flatband is partially filled. It indicates that we can explore magnetism that is purely orbital in the TBG.

*Note added.* Recently, we became aware of the work of Mao *et al.* [70], which reported evidence of the correlated states in strain-induced flatbands in graphene monolayer. We also became aware of the work of Tschirhart *et al.* [71], which showed the orbital magnetism of several  $\mu_B$  per electron in the magic-angle TBG via a superconducting quantum interference device.

This work was supported by the National Natural Science Foundation of China (Grants No. 11974050 and No. 11674029) and National Key R&D Program of China (Grant No. 2017YFA0303301). L.H. also acknowledges support from the National Program for Support of Top-notch Young Professionals, support from “Fundamental Research Funds for the Central Universities,” and support from “Chang Jiang Scholars Program.”

- 
- [1] J. M. B. Lopes dos Santos, N. M. R. Peres, and A. H. Castro Neto, Graphene Bilayer with a Twist: Electronic Structure, *Phys. Rev. Lett.* **99**, 256802 (2007).
  - [2] G. Li, A. Luican, J. M. B. Lopes dos Santos, A. H. Castro Neto, A. Reina, J. Kong, and E. Y. Andrei, Observation of Van Hove singularities in twisted graphene layers, *Nat. Phys.* **6**, 109 (2009).
  - [3] W. Yan, M. Liu, R.-F. Dou, L. Meng, L. Feng, Z.-D. Chu, Y. Zhang, Z. Liu, J.-C. Nie, and L. He, Angle-Dependent Van Hove Singularities in a Slightly Twisted Graphene Bilayer, *Phys. Rev. Lett.* **109**, 126801 (2012).
  - [4] A. Luican, G. Li, A. Reina, J. Kong, R. R. Nair, K. S. Novoselov, A. K. Geim, and E. Y. Andrei, Single-Layer Behavior and Its Breakdown in Twisted Graphene Layers, *Phys. Rev. Lett.* **106**, 126802 (2011).
  - [5] I. Brihuega, P. Mallet, H. Gonzalez-Herrero, G. T. de Laissardiere, M. M. Ugeda, L. Magaud, J. M. Gomez-Rodriguez, F. Yndurain, and J.-Y. Veuillen, Unraveling the Intrinsic and Robust Nature of van Hove Singularities in Twisted Bilayer Graphene by Scanning Tunneling Microscopy and Theoretical Analysis, *Phys. Rev. Lett.* **109**, 196802 (2012).
  - [6] T. Ohta, J. T. Robinson, P. J. Feibelman, A. Bostwick, E. Rotenberg, and T. E. Beechem, Evidence for Interlayer Coupling and Moiré Periodic Potentials in Twisted Bilayer Graphene, *Phys. Rev. Lett.* **109**, 186807 (2012).
  - [7] R. Bistritzer and A. H. MacDonald, Moiré bands in twisted double-layer graphene, *Proc. Natl. Acad. Sci. USA* **108**, 12233 (2011).
  - [8] P. San-Jose, J. Gonzalez, and F. Guinea, Non-Abelian Gauge Potentials in Graphene Bilayers, *Phys. Rev. Lett.* **108**, 216802 (2012).
  - [9] E. S. Morell, J. D. Correa, P. Vargas, M. Pacheco, and Z. Barticevic, Flat bands in slightly twisted bilayer graphene: Tight-binding calculations, *Phys. Rev. B* **82**, 121407(R) (2010).
  - [10] L.-J. Yin, J.-B. Qiao, W.-J. Zuo, W.-T. Li, and L. He, Experimental evidence for non-Abelian gauge potentials in twisted graphene bilayers, *Phys. Rev. B* **92**, 081406(R) (2015).
  - [11] Y. Cao, V. Fatemi, A. Demir, S. Fang, S. L. Tomarken, J. Y. Luo, J. D. Sanchez-Yamagishi, K. Watanabe, T. Taniguchi, E. Kaxiras, R. C. Ashoori, and P. Jarillo-Herrero, Correlated insulator behaviour at half-filling in magic-angle graphene superlattices, *Nature (London)* **556**, 80 (2018).
  - [12] Y. Cao, V. Fatemi, S. Fang, K. Watanabe, T. Taniguchi, E. Kaxiras, and P. Jarillo-Herrero, Unconventional superconductivity in magic-angle graphene superlattices, *Nature (London)* **556**, 43 (2018).
  - [13] M. Yankowitz, S. Chen, H. Polshyn, Y. Zhang, K. Watanabe, T. Taniguchi, D. Graf, A. F. Young, and C. R. Dean, Tuning superconductivity in twisted bilayer graphene, *Science* **363**, 1059 (2019).
  - [14] X. Lu, P. Stepanov, W. Yang, M. Xie, M. A. Aamir, I. Das, C. Urgell, K. Watanabe, T. Taniguchi, G. Zhang, A. Bachtold, A. H. MacDonald, and D. K. Efetov, Superconductors, orbital magnets, and correlated states in magic angle bilayer graphene, *Nature (London)* **574**, 653 (2019).
  - [15] A. L. Sharpe, E. J. Fox, A. W. Barnard, J. Finney, K. Watanabe, T. Taniguchi, M. A. Kastner, and D. Goldhaber-Gordon, Emergent ferromagnetism near three-quarters filling in twisted bilayer graphene, *Science* **365**, 605 (2019).
  - [16] M. Serlin, C. L. Tschirhart, H. Polshyn, Y. Zhang, J. Zhu, K. Watanabe, T. Taniguchi, and A. F. Young, Intrinsic quantized

- anomalous Hall effect in a moiré superlattice, *Science* **367**, 900 (2020).
- [17] M. A. H. Vozmediano, M. I. Katsnelson, and F. Guinea, Gauge fields in graphene, *Phys. Rep.* **496**, 109 (2010).
- [18] F. Guinea, M. I. Katsnelson, and M. A. H. Vozmediano, Midgap states and charge inhomogeneities in corrugated graphene, *Phys. Rev. B* **77**, 075422 (2008).
- [19] F. Guinea, B. Horowitz, and P. Le Doussal, Gauge field induced by ripples in graphene, *Phys. Rev. B* **77**, 205421 (2008).
- [20] N. Levy, S. A. Burke, K. L. Meaker, M. Panlasigui, A. Zettl, F. Guinea, A. H. Castro Neto, and M. F. Crommie, Strain-induced pseudo-magnetic fields greater than 300 Tesla in graphene nanobubbles, *Science* **329**, 544 (2010).
- [21] W. Yan, W.-Y. He, Z.-D. Chu, M. Liu, L. Meng, R.-F. Dou, Y. Zhang, Z. Liu, J.-C. Nie, and L. He, Strain and curvature induced evolution of electronic band structures in twisted graphene bilayer, *Nat. Commun.* **4**, 2159 (2013).
- [22] L. Meng, W.-Y. He, H. Zheng, M. Liu, H. Yan, W. Yan, Z.-D. Chu, K. K. Bai, R.-F. Dou, Y. Zhang, Z. Liu, J.-C. Nie, and L. He, Strain-induced one-dimensional Landau level quantization in corrugated graphene, *Phys. Rev. B* **87**, 205405 (2013).
- [23] H. Yan, Y. Sun, L. He, J.-C. Nie, and M. H. W. Chan, Observation of Landau-level-like quantization at 77 K along a strained-induced graphene ridge, *Phys. Rev. B* **85**, 035422 (2012).
- [24] S.-Y. Li, K.-K. Bai, L.-J. Yin, J.-B. Qiao, W.-X. Wang, and L. He, Observation of unconventional splitting of Landau levels in strained graphene, *Phys. Rev. B* **92**, 245302 (2015).
- [25] D. Guo, T. Kondo, T. Machida, K. Iwatake, S. Okada, and J. Nakamura, Observation of Landau levels in potassium-intercalated graphite under a zero magnetic field, *Nat. Commun.* **3**, 1068 (2012).
- [26] J. Lu, A. H. Castro Neto, and K. P. Loh, Transforming moiré blisters into geometric graphene nano-bubbles, *Nat. Commun.* **3**, 823 (2012).
- [27] A. Georgi, P. Nemes-Incze, R. Carrillo-Bastos, D. Faria, S. V. Kusminski, D. Zhai, M. Schneider, D. Subramaniam, T. Mashoff, N. M. Freitag, M. Liebmann, M. Pratzler, L. Wirtz, C. R. Woods, R. V. Gorbachev, Y. Cao, K. S. Novoselov, N. Sandler, and M. Morgenstern, Tuning the pseudospin polarization of graphene by a pseudomagnetic field, *Nano Lett.* **17**, 2240 (2017).
- [28] Y. Jiang, J. Mao, J. Duan, X. Lai, K. Watanabe, T. Taniguchi, and E. Y. Andrei, Visualizing strain-induced pseudomagnetic fields in graphene through a hBN magnifying glass, *Nano Lett.* **17**, 2839 (2017).
- [29] Y. Liu, J. N. B. Rodrigues, Y. Z. Luo, L. Li, A. Carvalho, M. Yang, E. Laksono, J. Lu, Y. Bao, H. Xu, S. J. R. Tan, Z. Qiu, C. H. Sow, Y. P. Feng, A. H. Castro Neto, S. Adam, J. Lu, and K. P. Loh, Tailoring sample-wide pseudo-magnetic fields on a graphene-black phosphorus heterostructure, *Nat. Nanotechnol.* **13**, 828 (2018).
- [30] Z. Bi, N. F. Q. Yuan, and L. Fu, Designing flat bands by strain, *Phys. Rev. B* **100**, 035448 (2019).
- [31] P. Jia, W. Chen, J. Qiao, M. Zhang, X. Zheng, Z. Xue, R. Liang, C. Tian, L. He, Z. Di, and X. Wang, Programmable graphene nanobubbles with three-fold symmetric pseudo-magnetic fields, *Nat. Commun.* **10**, 3127 (2019).
- [32] S.-Y. Li, Y. Su, Y.-N. Ren, and L. He, Valley Polarization and Inversion in Strained Graphene via Pseudo-Landau Levels, Valley Splitting of Real Landau Levels and Confined States, *Phys. Rev. Lett.* **124**, 106802 (2020).
- [33] F. Guinea, M. I. Katsnelson, and A. K. Geim, Energy gaps and a zero-field quantum Hall effect in graphene by strain engineering, *Nat. Phys.* **6**, 30 (2010).
- [34] K. K. Gomes, W. Mar, W. Ko, F. Guinea, and H. C. Manoharan, Designer Dirac fermions and topological phases in molecular graphene, *Nature (London)* **483**, 306 (2012).
- [35] C. Hsu, M. L. Teague, J. Wang, and N. Yeh, Nanoscale strain engineering of giant pseudo-magnetic fields, valley polarization, and topological channels in graphene, *Sci. Adv.* **6**, eaat9488 (2020).
- [36] F. Xu, P. Chou, C. Chung, T. Lee, and C. Mou, Strain-induced superconducting pair density wave states in graphene, *Phys. Rev. B* **98**, 205103 (2018).
- [37] L. Huder, A. Artaud, T. L. Quang, G. T. de Laissardière, A. G. M. Jansen, G. Lapertot, C. Chapelier, and V. T. Renard, Electronic Spectrum of Twisted Graphene Layers under Heterostrain, *Phys. Rev. Lett.* **120**, 156405 (2018).
- [38] C. Yan, D.-L. Ma, J.-B. Qiao, H.-Y. Zhong, L. Yang, S.-Y. Li, Z.-Q. Fu, Y. Zhang, and L. He, Scanning tunneling microscopy study of the quasicrystalline 30° twisted bilayer graphene, *2D Mater.* **6**, 045041 (2019).
- [39] Y.-W. Liu, J.-B. Qiao, C. Yan, Y. Zhang, S.-Y. Li, and L. He, Magnetism near half-filling of a Van Hove singularity in twisted graphene bilayer, *Phys. Rev. B* **99**, 201408(R) (2019).
- [40] See Supplemental Material at <http://link.aps.org/supplemental/10.1103/PhysRevB.102.081403> for more experimental data, analysis, and discussion.
- [41] Y. Xie, B. Lian, B. Jack, X. Liu, C.-L. Chiu, K. Watanabe, T. Taniguchi, B. A. Bernevig, and A. Yazdani, Spectroscopic signatures of many-body correlations in magic-angle twisted bilayer graphene, *Nature (London)* **572**, 101 (2019).
- [42] A. Kerelsky, L. J. McGilly, D. M. Kennes, L. Xian, M. Yankowitz, S. Chen, K. Watanabe, T. Taniguchi, J. Hone, C. Dean, A. Rubio, and A. N. Pasupathy, Maximized electron interactions at the magic angle in twisted bilayer graphene, *Nature (London)* **572**, 95 (2019).
- [43] Y. Jiang, X. Lai, K. Watanabe, T. Taniguchi, K. Haule, J. Mao, and E. Y. Andrei, Charge-order and broken rotational symmetry in magic angle twisted bilayer graphene, *Nature (London)* **573**, 91 (2019).
- [44] Y. Choi, J. Kemmer, Y. Peng, A. Thomson, H. Arora, R. Polski, Y. Zhang, H. Ren, J. Alicea, G. Refael, F. van Oppen, K. Watanabe, T. Taniguchi, and S. Nadj-Perge, Electronic correlations in twisted bilayer graphene near the magic angle, *Nat. Phys.* **15**, 1174 (2019).
- [45] J.-B. Qiao, L.-J. Yin, and L. He, Twisted graphene bilayer around the first magic angle engineered by heterostrain, *Phys. Rev. B* **98**, 235402 (2018).
- [46] H. Shi, Z. Zhang, Z. Qi, K. Huang, E. Van Veen, J. A. Silva-Guillen, R. Zhang, P. Li, K. Xie, H. Ji, M. I. Katsnelson, S. Yuan, S. Qin, and Z. Zhang, Large-area, periodic, and tunable intrinsic pseudo-magnetic fields in low-angle twisted bilayer graphene, *Nat. Commun.* **11**, 371 (2020).
- [47] W. Bao, F. Miao, Z. Chen, H. Zhang, W. Jang, C. Dames, and C. N. Lau, Controlled ripple texturing of suspended graphene and ultrathin graphite membranes, *Nat. Nanotechnol.* **4**, 562 (2009).

- [48] C. Wu, D. Bergman, L. Balents, and S. D. Sarma, Flat Bands and Wigner Crystallization in the Honeycomb Optical Lattice, *Phys. Rev. Lett.* **99**, 070401 (2007).
- [49] E. H. Hwang and S. D. Sarma, Dielectric function, screening, and plasmons in two-dimensional graphene, *Phys. Rev. B* **75**, 205418 (2007).
- [50] A. Luican-Mayer, M. Kharitonov, G. Li, C. Lu, I. Skachko, A. B. Gonçalves, K. Watanabe, T. Taniguchi, and E. Y. Andrei, Screening Charged Impurities and Lifting the Orbital Degeneracy in Graphene by Populating Landau Levels, *Phys. Rev. Lett.* **112**, 036804 (2014).
- [51] J. Kang and O. Vafek, Strong Coupling Phases of Partially Filled Twisted Bilayer Graphene Narrow Bands, *Phys. Rev. Lett.* **122**, 246401 (2019).
- [52] S. Kim, J. Schwenk, D. Walkup, Y. Zeng, F. Ghahari, S. T. Le, M. R. Slot, J. Berwanger, S. R. Blankenship, K. Watanabe *et al.*, Edge channels of broken-symmetry quantum Hall states in graphene probed by atomic force microscopy, [arXiv:2006.10730](https://arxiv.org/abs/2006.10730).
- [53] A. F. Young, C. R. Dean, L. Wang, H. Ren, P. Cadden-Zimansky, K. Watanabe, T. Taniguchi, J. Hone, K. L. Shepard, and P. Kim, Spin and valley quantum Hall ferromagnetism in graphene, *Nat. Phys.* **8**, 550 (2012).
- [54] S.-Y. Li, Y. Zhang, L.-J. Yin, and L. He, Scanning tunneling microscope study of quantum Hall isospin ferromagnetic states in the zero Landau level in a graphene monolayer, *Phys. Rev. B* **100**, 085437 (2019).
- [55] B. L. Chittari, G. Chen, Y. Zhang, F. Wang, and J. Jung, Gate-Tunable Topological Flat Bands in Trilayer Graphene Boron-Nitride Moiré Superlattices, *Phys. Rev. Lett.* **122**, 016401 (2019).
- [56] R. T. Weitz, M. T. Allen, B. E. Feldman, J. Martin, and A. Yacoby, Broken-symmetry states in doubly gated suspended bilayer graphene, *Science* **330**, 812 (2010).
- [57] R. Nandkishore and L. Levitov, Dynamical Screening and Excitonic Instability in Bilayer Graphene, *Phys. Rev. Lett.* **104**, 156803 (2010).
- [58] N. Bultinck, S. Chatterjee, and M. P. Zaletel, Mechanism for Anomalous Hall Ferromagnetism in Twisted Bilayer Graphene, *Phys. Rev. Lett.* **124**, 166601 (2020).
- [59] J. Liu, Z. Ma, J. Gao, and X. Dai, Quantum Valley Hall Effect, Orbital Magnetism, and Anomalous Hall Effect in Twisted Multilayer Graphene Systems, *Phys. Rev. X* **9**, 031021 (2019).
- [60] J. Liu and X. Dai, Correlated insulating states and the quantum anomalous Hall phenomena at all integer fillings in twisted bilayer graphene, [arXiv:1911.03760](https://arxiv.org/abs/1911.03760).
- [61] C. Repellin, Z. Dong, Y. Zhang, and T. Senthil, Ferromagnetism in Narrow Bands of Moiré Superlattices, *Phys. Rev. Lett.* **124**, 187601 (2020).
- [62] M. Xie and A. H. MacDonald, Nature of the Correlated Insulator States in Twisted Bilayer Graphene, *Phys. Rev. Lett.* **124**, 097601 (2020).
- [63] Z. Song, Z. Wang, W. Shi, G. Li, C. Fang, and B. A. Bernevig, All Magic Angles in Twisted Bilayer Graphene are Topological, *Phys. Rev. Lett.* **123**, 036401 (2019).
- [64] B. Lian, F. Xie, and B. A. Bernevig, The Landau level of fragile topology, *Phys. Rev. B* **102**, 041402(R) (2020).
- [65] Y.-H. Zhang, D. Mao, and T. Senthil, Twisted bilayer graphene aligned with hexagonal boron nitride: Anomalous hall effect and a lattice model, *Phys. Rev. Research* **1**, 033126 (2020).
- [66] N. Bultinck, E. Khalaf, S. Liu, S. Chatterjee, A. Vishwanath, and M. P. Zaletel, Ground State and Hidden Symmetry of Magic Angle Graphene at Even Integer Filling, *Phys. Rev. X* **10**, 031034 (2020).
- [67] J. Cao, F. Qi, H. Yang, and G. Jin, Monolayer-gap modulated topological phases in twisted bilayer graphene, *Phys. Rev. B* **101**, 155419 (2020).
- [68] P. Stepanov, I. Das, X. Lu, A. Fahimniya, K. Watanabe, T. Taniguchi, F. H. L. Koppens, J. Lischner, L. Levitov, and D. K. Efetov, Untying the insulating and superconducting orders in magic-angle graphene, *Nature* **583**, 375 (2020).
- [69] W.-Y. He, D. Goldhaber-Gordon, and K. T. Law, Giant orbital magnetoelectric effect and current-induced magnetization switching in twisted bilayer graphene, *Nat. Commun.* **11**, 1650 (2020).
- [70] J. Mao, S. P. Milovanovic, M. Andelkovic, X. Lai, Y. Cao, K. Watanabe, T. Taniguchi, L. Covaci, F. M. Peeters, A. K. Geim, Y. Jiang, and E. Y. Andrei, Evidence of flat bands and correlated states in buckled graphene superlattices, *Nature* **584**, 215 (2020).
- [71] C. L. Tschirhart, M. Serlin, H. Polshyn, A. Shragai, Z. Xia, J. Zhu, Y. Zhang, K. Watanabe, T. Taniguchi, M. E. Huber, and A. F. Young, Imaging orbital ferromagnetism in a moiré Chern insulator, [arXiv:2006.08053](https://arxiv.org/abs/2006.08053).